Bioactive Materials 19 (2023) 703–716

Contents lists available at ScienceDirect

Bioactive Materials

journal homepage: www.keaipublishing.com/en/journals/bioactive-materials

Robust hydrogel adhesives for emergency rescue and gastric perforation repair

Jing Yu [a], Yanyang Qin [a], Yuxuan Yang [b], Xiaodan Zhao [b], Zixi Zhang [c], Qiang Zhang [a], Yaqiong Su [a], Yanfeng Zhang [a], Yilong Cheng [a,*]

[a] School of Chemistry, Xi'an Jiaotong University, Xi'an, 710049, China
[b] Key Laboratory of Shaanxi Province for Craniofacial Precision Medicine Research, College of Stomatology, Xi'an Jiaotong University, Xi'an, 710049, China
[c] Department of Dermatology, The First Affiliated Hospital of Xi'an Jiaotong University, Xi'an Jiaotong University, Xi'an, 710061, China

ARTICLE INFO

Keywords:
Adhesive hydrogel
Hydrogen bond
Amino acid
Emergency rescue
Gastric perforation repair

ABSTRACT

Development of biocompatible hydrogel adhesives with robust tissue adhesion to realize instant hemorrhage control and injury sealing, especially for emergency rescue and tissue repair, is still challenging. Herein, we report a potent hydrogel adhesive by free radical polymerization of *N*-acryloyl aspartic acid (AASP) in a facile and straightforward way. Through delicate adjustment of steric hindrance, the synergistic effect between interface interactions and cohesion energy can be achieved in PAASP hydrogel verified by X-ray photoelectron spectroscopy (XPS) analysis and simulation calculation compared to poly (*N*-acryloyl glutamic acid) (PAGLU) and poly (*N*-acryloyl amidomalonic acid) (PAAMI) hydrogels. The adhesion strength of the PAASP hydrogel could reach 120 kPa to firmly seal the broken organs to withstand the external force with persistent stability under physiological conditions, and rapid hemostasis in different hemorrhage models on mice is achieved using PAASP hydrogel as physical barrier. Furthermore, the paper-based Fe^{3+} transfer printing method is applied to construct PAASP-based Janus hydrogel patch with both adhesive and non-adhesive surfaces, by which simultaneous wound healing and postoperative anti-adhesion can be realized in gastric perforation model on mice. This advanced hydrogel may show vast potential as bio-adhesives for emergency rescue and tissue/organ repair.

1. Introduction

Adhesive hydrogels have gained increasing attention in wound dressing, tissue repair, drug delivery, and intelligent wearable electronics because of their excellent biocompatibility and tissue resemblance [1–4]. It has been reported that two prerequisites are required for hydrogels to achieve strong and stable adhesion: the hydrogels should form robust interactions with the substrate interface; an effective energy dissipation mechanism should exist in the hydrogels which can dissipate energy when subjected to external forces [5–7]. Due to structural heterogeneity or lack of energy dissipation mechanism, traditional hydrogels are usually mechanically weak. Although the recently developed double-network hydrogels, nanocomposite hydrogels, and topological hydrogels exhibit excellent mechanical properties [8–11], the increase of crosslinking density restricts the movement of polymer chains, thus affecting the interactions with the adhesion interface [12]. Hence, it remains a great challenge to realize the synergistic effect between the interface bonding force and toughness in the bulk hydrogel.

In general, adhesive hydrogels as surgical sealants for wound closure and tissue repair must meet several basic conditions. First of all, the hydrogels need to exhibit appropriate adhesion strength to achieve a strong sealing effect. Fibrin adhesives were commonly used as surgical sealants because of their good biocompatibility [13]. However, their applications were constrained by low adhesion strength and high cost. The mechanical properties of most hydrogels would decline dramatically due to network swelling when exposed to the aqueous environment for a long time, further resulting in the loss of adhesion strength [14,15]. Therefore, hydrogels should possess adhesion stability under physiological conditions. Besides, the ideal hydrogel tissue adhesives should have appropriate mechanical properties similar to tissues, including toughness, elasticity, and recovery properties, in order to withstand dynamic loading during repair process. In addition, good biocompatibility is also of the essence. Cyanoacrylate-based adhesives exhibit strong adhesion behavior; however, they suffer from biotoxicity induced

Peer review under responsibility of KeAi Communications Co., Ltd.
* Corresponding author.
E-mail address: yilongcheng@mail.xjtu.edu.cn (Y. Cheng).

https://doi.org/10.1016/j.bioactmat.2022.05.010
Received 9 January 2022; Received in revised form 14 April 2022; Accepted 6 May 2022

by degraded products [16]. Considering the possibility of postoperative adhesion using the two-sided tissue adhesives during surgery, it is necessary to design Janus hydrogel patches in order to achieve tissue repair and anti-adhesion effect simultaneously, in which one side can adhere to the damaged tissue for repair and the other side act as a physical barrier for the prevention of postoperative adhesion [17]. Moreover, the adhesive hydrogels should feature specific properties based on the physiological environment, tissue histopathology, and surgical procedure [18,19]. For example, excellent acid resistance should be achieved for the adhesive hydrogels used in gastric

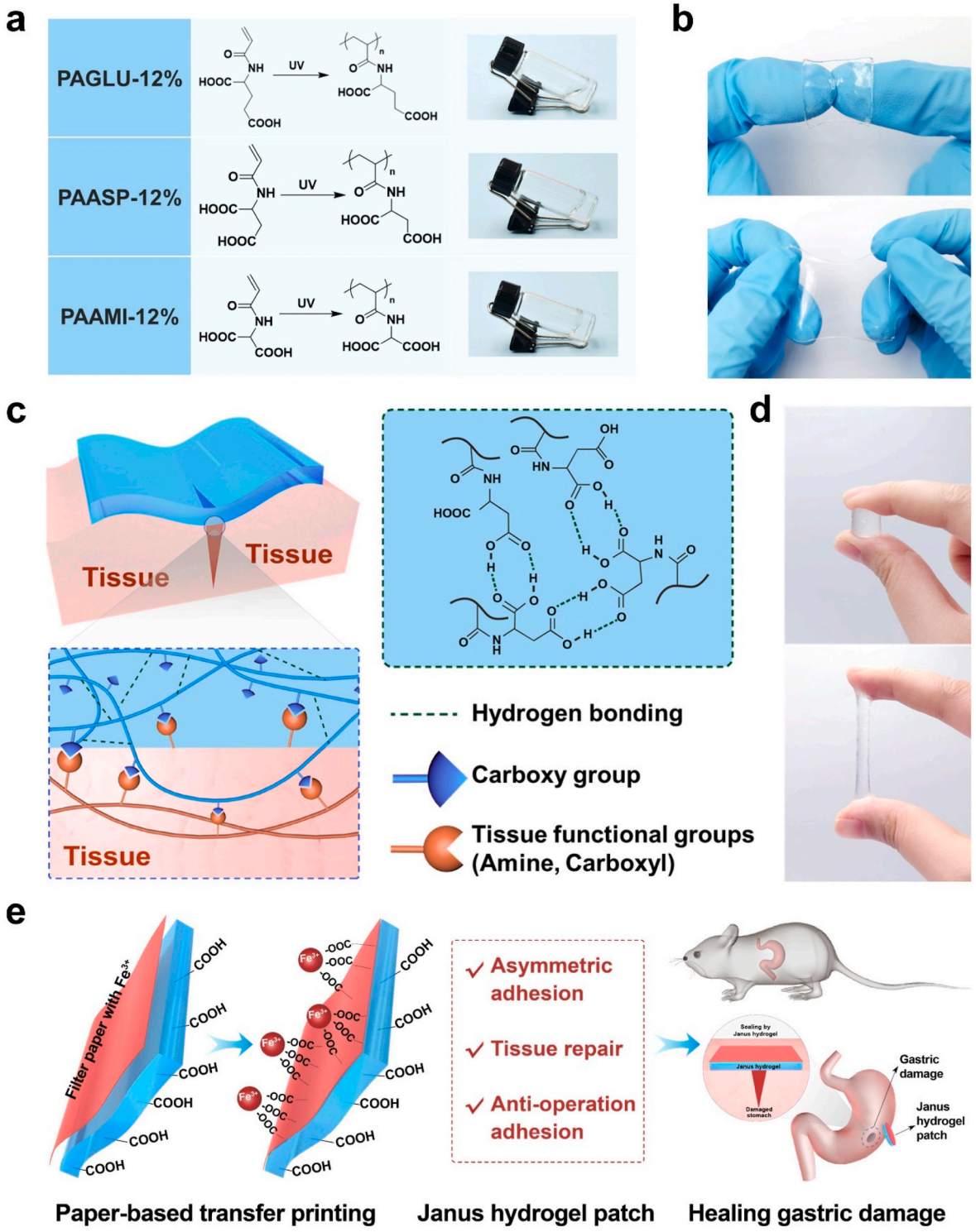

Fig. 1. The design strategy and application prospect of the adhesive hydrogel. (a) Synthetic routes of PAGLU, PAASP, and PAAMI and the corresponding photographs of PAGLU-12%, PAASP-12%, and PAAMI-12% in aqueous solution. (b) Photographs of PAASP-35% hydrogel under extension. (c) Schematic overview of PAASP hydrogel adhesion to tissue: adhesion interface and the hydrogel matrix containing hydrogen bond crosslinked network. (d) Photographs of PAASP-35% hydrogel strongly adhered to fingers subjected to large stretch. (e) Schematic illustrations of Janus hydrogel patch prepared by paper-based Fe^{3+} transfer printing and its application in gastric perforation repair.

perforation repair.

In recent years, most research has been focused on the development of hydrogel-based bio-adhesives, mainly inspired by mussel adhesive proteins [20–22]. The catechol groups in the mussel adhesive proteins can interact with the targeting interfaces through hydrogen bonding, coordination, and π-π stacking [23,24]. However, such catechol-based adhesive hydrogels, which are usually synthesized under alkaline conditions through oxidative polymerization, exhibit obvious disadvantages. The uncontrollable oxidation process leads to the decrease of the phenolic hydroxyl groups, thus reducing the adhesion strength [20]. Besides, the hydrogels are primarily designed by grafting molecules with catechol structure onto biocompatible macromolecules such as chitosan, hyaluronic acid, and poly(ethylene glycol) [25–28]. Unfortunately, its preparation relies on complex design and expensive reagents, which is time-consuming and high-cost, limiting large-scale production. Therefore, it is urgent to develop hydrogel-based tissue adhesives with stable adhesion, excellent mechanical properties, good biocompatibility, and strong adaptability through simple and economical methods for the applications in clinic.

Hydrogen bond, as one of the most common non-covalent bonds, could endow materials with high toughness, elasticity, and recovery properties owing to its dynamic nature [29,30]. As the basic structural unit of proteins, amino acids play a vital role in the formation of the secondary structure of protein through hydrogen bonds. It has been reported that amino acid derivatives, which can form intermolecular multiple hydrogen bond interactions, have the advantage of constructing hydrogels with comprehensive mechanical properties after being introduced into polymer design [31,32]. Owing to the presence of carboxyl groups on amino acids, the resulting hydrogels also present the potential as adhesives. Gao et al. reported a lysine-tackified hydrogel with adhesiveness towards various substrates and explored the applications in wearable sensors, in which the pendant carboxyl group could form hydrogen bonding with human skin tissue [33]. Liu et al. designed an instant adhesive poly (*N*-acryloyl 2-glycine)/hydroxyapatite organic-inorganic hybrid hydrogel for self-rescue in emergencies [12]. The polymer chains were adsorbed on the surface of nanoparticles, which was conducive to exposing more carboxyl groups to achieve high adhesion. However, the adhesion strength of hydrogels was strongly dependent on the interactions between polymer chains and nanoparticles. Thus, the ratio between the two components was required to be precisely regulated.

It is assumed that amino acid derivatives with bi-carboxyl groups may exhibit stronger adhesion owing to more free carboxyl groups interacting with the adhesion interface without the assistance of other components. In this work, we employed three bi-carboxyl-included vinyl monomers, *N*-acryloyl glutamic acid (AGLU), *N*-acryloyl aspartic acid (AASP), and *N*-acryloyl amidomalonic acid (AAMI), to construct adhesive hydrogels with comprehensive mechanical properties and robust adhesiveness. The hydrogels were prepared by one-pot free radical polymerization of these three derivatives. It was observed in Fig. 1a that the viscosity of the PAGLU, PAASP, and PAAMI aqueous solutions (the monomer concentration was 12 wt%) increased successively. We hypothesize that there exists a more compact hydrogen bond cross-linking network in PAAMI. Further increasing the monomer concentration to 35%, the PAASP hydrogel exhibited outstanding mechanical properties, especially excellent flexibility (Fig. 1b). We speculate that carboxyl groups on the side chains of PAASP not only participate in the formation of multiple hydrogen bonds to construct the hydrogel network but also form strong hydrogen bond interactions with the polar groups on the tissue interface, thus showing strong adhesion to biological tissues (Fig. 1c and d).

Further results conclusively showed that the PAASP hydrogel was integrated with good toughness, robust elasticity, fatigue resistance, and strong adhesion to various materials. We also established *in vitro* porcine organ models (incision on stomach, bladder, intestine, and trachea) to confirm the potential for emergency rescue. *In vitro* cell experiments, subcutaneous implantation test, and *in vivo* hemostasis tests proved that the PAASP hydrogel possessed good biocompatibility and rapid hemostasis ability. Considering the complex internal environment, we also evaluated the adhesion stability of the PAASP hydrogel versus incubation time in water, physiological saline, PBS, and simulated gastric fluid at 37 °C. To prevent the PAASP hydrogel patch from causing peritoneal adhesion in the process of *in vivo* tissue repair, we prepared a Janus hydrogel patch with both adhesive surface and non-adhesive surface by means of paper-based Fe^{3+} transfer printing (Fig. 1e) [34,35]. The Janus hydrogel patch was employed for the treatment of gastric perforation on mice, and the results indicated that the hydrogel could realize tissue repair and anti-postoperative adhesion simultaneously.

2. Materials and methods

2.1. Materials

Glutamic acid (GLU), aspartic acid (ASP), diethyl aminomalonate hydrochloride, and acryloyl chloride were supplied by Adamas-beta Co., Ltd. 2-Hydroxy-4'-(2-hydroxyethoxy)-2-methyl-propiophe (IRGACURE 2959, 98%) were provided by TCI (Shanghai) Chemical Industry Co., Ltd.. All other chemicals and solvents used were analytical grade without further purification.

2.2. Preparation of poly(N-acryloyl aspartic acid) (PAASP) hydrogel

The PAGLU, PAASP, and PAAMI hydrogels were prepared through photo-initiated free radical polymerization of the corresponding vinyl monomers with different concentrations in water. The detailed preparation method can be found in the Supplementary Material.

2.3. Preparation of PAASP-35%/Fe^{3+} Janus hydrogel patch

The filter paper was first cut into the size of the hydrogel. Then the filter paper was soaked in 0.06 M $FeCl_3$ solution for a few seconds and subsequently placed on one side of PAASP-35% hydrogel for 30 s. Finally, the suspension on the surface of the hydrogel was wiped off with a clean filter paper.

2.4. Porcine organ sealing test

Porcine organs, including stomach, bladder, small intestine, and trachea, were obtained from the slaughterhouse. The PAASP-35% hydrogel for organ sealing was prepared as a sheet structure with 2 cm in length and 2 cm in width. For ease of operation, we attached PTFE sheets ($2.5 \times 2.5 \times 0.1$ cm^3) to the back of the hydrogel. As for the isolated porcine stomach model, we first made a 5 mm incision on the stomach with a scalpel, and then adhered the hydrogel patch to the incision for sealing. Finally, tap water was infused into the stomach to examine the sealing effect. The sealing of porcine bladder and small intestine was conducted in the same way. After sealing the trachea with a hydrogel patch, the trachea connected to the lung lobes was placed in water, and the air was pumped through an electromagnetic air pump to check the sealing result.

2.5. In vivo repairment of gastric damage with PAASP-35%/Fe^{3+} Janus hydrogel patch

All animal experiments in this study were approved by the Ethics Committee of Xi'an Jiaotong University. All surgical instruments were sterilized at high temperature before the operation. Eight SD rats were randomly divided into two groups. The rats were anesthetized with sodium pentobarbital (50 mg kg^{-1}), and then the abdomens of the rats were shaved by shaver and disinfected with iodophor. After the abdominal cavity was exposed, a 0.5 cm incision was made on the stomach with a scalpel and the outflowing gastric contents were gently

wiped off with a sterile cotton swab. A circular PAASP-35%/Fe^{3+} Janus hydrogel patch with a diameter of 1 cm was then immediately adhered to the incision. The control group was treated with surgical sutures. The healing effect of the gastric damage was recorded seven days after surgery, and the gastric tissue was collected and fixed for further H&E staining analysis.

2.6. Statistical analysis

The *In vivo* hemostatic test result was presented as mean ± standard deviation and analyzed by Shapiro-Wilk test followed by Student's *t*-test, in which $P < 0.05$ was considered statistical significance. GraphPad Prism software (GraphPad Software Inc.) was used for data analysis.

3. Results and discussion

3.1. Comparison of PAGLU, PAASP, and PAAMI hydrogels

For comparison, three bi-carboxyl-included acrylamide monomers, AGLU (glutamic acid derivative), AASP (aspartic acid derivative), and AAMI, were synthesized with minor modifications to the previously described method [32]. The ^{1}H NMR spectra shown in Figs. S1–S3 confirmed the successful synthesis of the three monomers. Correspondingly, PAGLU, PAASP, and PAAMI hydrogels were prepared by photo-irradiated one-pot radical polymerization of the monomer aqueous solutions with different concentrations. The Fourier transform infrared (FTIR) spectroscopy was conducted to monitor the polymerization process. As shown in Fig. S4, the peak at 1624 cm^{-1} assigned to the acryloyl double bond disappeared completely after 20 min, indicating that the polymerization was accomplished. The resulting hydrogels were named PAGLU-X, PAASP-X, and PAAMI-X, where X represented the monomer concentration in weight percentage.

The uniaxial tensile test was performed to characterize the mechanical properties of PAGLU-35%, PAASP-35%, and PAAMI-35% hydrogels (Fig. 2a). We found that the tensile strength and the elongation at break of these three hydrogels were in the range of 30–73 kPa and 920–1700%, respectively. Fig. 2b displayed a brief diagram of quantitative comparison of the tensile strength, maximum strain, Young's modulus, and toughness of PAGLU-35%, PAASP-35%, and PAAMI-35% hydrogels. It was observed that the PAASP-35% hydrogel exhibited the highest tensile strength, elongation at break, and toughness. Comparatively, the PAAMI-35% hydrogel showed the highest modulus. We assume that the steric hindrance of the methylene groups attached to the carboxyl groups plays a crucial role in the formation of hydrogen bonds and further affects the crosslinking density of the hydrogel network. For PAAMI hydrogel, the two carboxyl groups (COOH-1 and COOH-2, Table S1) were directly linked to the α-carbon atom, and thus both of them were involved in the formation of hydrogen bonds. With the increase of methylene groups between the α-carbon atom and COOH-2, there were fewer COOH-1 groups participating in the formation of hydrogen bonds due to steric hindrance. Hence, the modulus and the crosslinking density gradually decreased for PAAMI-35%, PAASP-35%, and PAGLU-35% hydrogels. As depicted in Fig. 2c, all three hydrogels showed three-dimensional interconnected porous network microstructures by scanning electron microscopy (SEM), and the smallest pore size and most compact structure were observed for PAAMI-35% hydrogel, which revealed its densest network induced by the elevated content of hydrogen bonds. Correspondingly, the number of free carboxyl groups should be relatively reduced. We further characterized the surface carboxyl group distribution of three hydrogels by X-ray photoelectron spectroscopy (XPS) analysis. It was observed from the C 1s spectrum that the PAGLU-35% hydrogel contained the highest content of C–OH and C=O, indicating that the most free carboxyl groups were present on the surface of the hydrogel. It further proved that few carboxyl groups were involved in the formation of hydrogen bonds due to the steric hindrance of the two methylene groups, which led to the lowest modulus for PAGLU-35% hydrogel. The density functional theory (DFT) calculations were also conducted to analyze the intermolecular H-bonding interaction energies in three hydrogels. Fig. 2e illustrated the optimized molecular models of double AGLU, AASP, and AAMI dimers. The dimer-dimer intermolecular hydrogen bonding interaction energies for AGLU, AASP, and AAMI are −42.6, −53.7, and −72.2 kJ mol^{-1}, respectively, indicating that the hydrogen-bonding interactions for double AGLU, AASP, and AAMI dimers are gradually enhanced. It could be observed from the optimized atomic structures that the least carboxyl group is involved in the formation of intermolecular hydrogen bonds between two AGLU dimers due to the influence of steric hindrance compared to AASP and AAMI dimers, which is consistent with our hypothesis.

3.2. Mechanical properties of PAASP hydrogels

After comparison, we found that the PAASP-35% hydrogel showed excellent mechanical properties (mechanical strength of 73 kPa, elongation at break of 1700%, and toughness of 0.52 MJ m^{-3}), which was comparable to the reported tough hydrogel adhesive [36]. It was presented in Fig. S5 that PAASP-35% hydrogel could withstand large stretching, knot stretching, crossover stretching, and twist stretching. The mechanical properties of the PAASP hydrogels with varied AASP monomer concentrations were further tested as shown in Fig. 3a. Generally, with the increment of monomer concentration, the tensile strength increased from 14 kPa to 118 kPa while the elongation at break declined from 2070% to 570%. This can be interpreted as higher hydrogen bond cross-linking density resulting in enhanced mechanical strength and network stiffness. Besides, the excellent stretchability may be attributed to the dissociation of the hydrogen bonds and macromolecular chain slippage caused by external forces [12]. It was noted that the tensile strength and elongation at break of PAASP-45% hydrogel were lower than that of PAASP-40% hydrogel. An explanation was that with 45% of AASP concentration the excessive hydrogen bond crosslinking network resulted in enhanced network stiffness and restricted movement of polymer chains, revealed by the significant increment of Young's modulus. In addition, the inhomogeneity of the network generated at higher crosslinking density also caused the decrease in mechanical strength. The detailed mechanical properties were summarized in Table S2. To further evaluate the toughness of the PAASP-35% hydrogel, cyclic tensile tests under different strains were conducted to examine the capability of energy dissipation (Fig. 3b). It was presented in Fig. 3c that the dissipated energy increased obviously at higher strain, which was attributed to the disruption of hydrogen bonds between molecular chains. Besides, we also conducted five successive loading-unloading tests to examine the anti-fatigue property of the PAASP-35% hydrogel. As illustrated in Fig. S6, the energy hysteresis almost overlapped after the first stretch cycle, indicating the rapid recovery and reconstruction of hydrogen bonds.

The compression and elastic recovery properties of the PAASP hydrogels were also characterized in detail. The compression stress of the PAASP hydrogels (Fig. 3d and e) increased from 0.37 to 4.46 MPa at 95% strain with the increase of AASP concentration, mainly due to the increase of hydrogen bonds mediated crosslinking density. It was observed in Fig. 3f that the PAASP-35% hydrogel could recover to its initial state after compression instantly. In order to further evaluate the compression recovery performance of the hydrogel, we carried out 50 consecutive cyclic compression tests at 80% strain on PAASP-35% hydrogel (Fig. 3g and h). The compressive stress-strain curves for all the cycles almost overlapped, and the maximum stress was basically unchanged, indicating that the PAASP-35% hydrogel exhibited robust elasticity and mechanical stability. It is encouraging that the reversible hydrogen bonding crosslinked network endows the PAASP-35% hydrogel with desirable mechanical properties required by bioadhesives. Especially, good elastic recovery performance is a prerequisite for hydrogels to be used as gastrointestinal sealants, which ensures

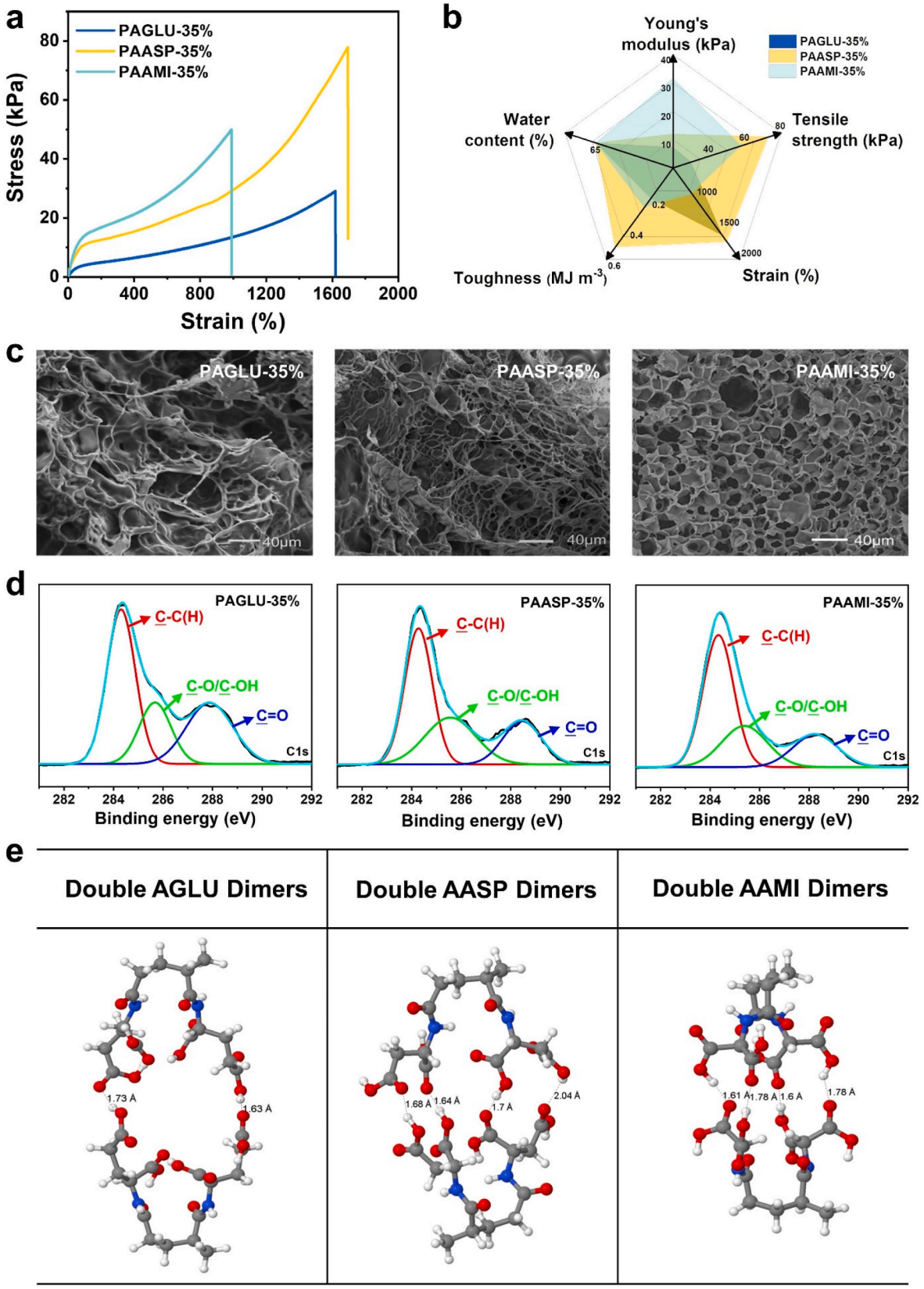

Fig. 2. Comparison between PAGLU-35%, PAASP-35%, and PAAMI-35% hydrogels. (a) Tensile stress-strain curves of PAGLU-35%, PAASP-35%, and PAAMI-35% hydrogels. (b) Comparison between PAGLU-35%, PAASP-35%, and PAAMI-35% hydrogels in terms of tensile strength, elongation at break, Young's modulus, and toughness. (c) SEM images of PAGLU-35%, PAASP-35%, and PAAMI-35% hydrogels. (d) Peak-fitting XPS spectra in the C1s regions of the surface of PAGLU-35%, PAASP-35%, and PAAMI-35% hydrogels. (e) The optimized conformation for double AGLU dimers, double AASP dimers, and double AAMI dimers. White, gray, blue, and red balls represent H, C, N, and O atoms, respectively. The dash lines denote hydrogen bonds.

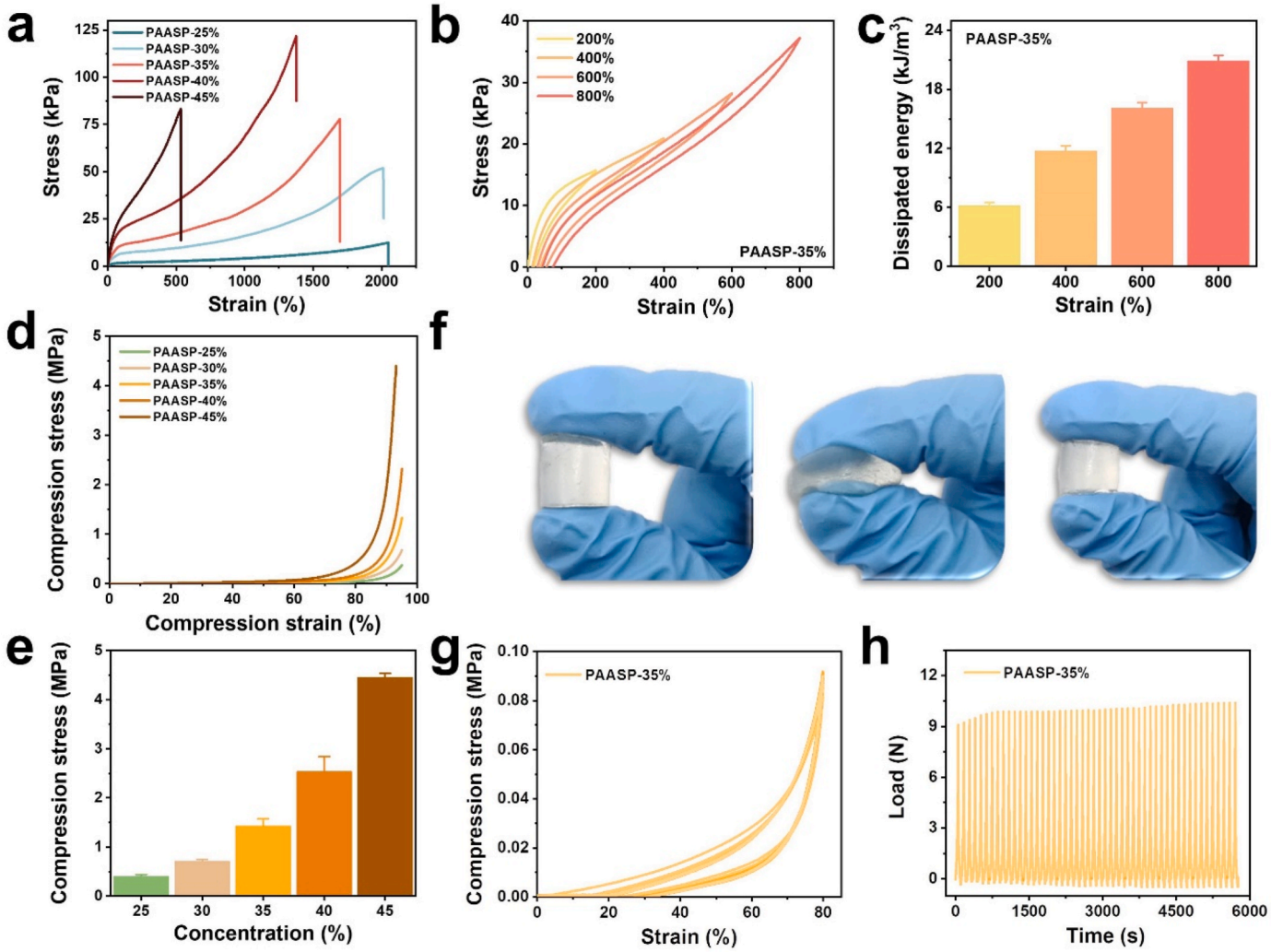

Fig. 3. Mechanical properties of PAASP hydrogels. (a) Tensile stress-strain curves of PAASP hydrogels with different monomer concentrations. (b) The loading-unloading curves and (c) the corresponding hysteresis loss of PAASP-35% hydrogel at different strains. (d) Compressive stress-strain curves and (e) the corresponding compression stress of PAASP hydrogels with different monomer concentrations at 95% strain. (f) Photographs showing the recovery of PAASP-35% hydrogel after compression. (g) The stress-strain curves and (h) the load-time curve of PAASP-35% hydrogel during 50 continuous compression cycles.

the tight adhesion to the repair area and allows for normal gastric peristalsis [18,37].

3.3. Adhesion properties of the PAASP hydrogels

It is reported that hydrogels with carboxyl groups showed adhesiveness with different substrates due to the formation of hydrogen bonds [12,33]. In this work, we found that the PAASP hydrogels displayed excellent adhesiveness to a large variety of materials. As presented in Fig. 4a, the PAASP-35% hydrogel could adhere to various biological tissues, such as muscle, lung, stomach, kidney, heart, and liver. Moreover, different kinds of organic and inorganic materials could also be adhered to the hydrogel (including iron, rubber, polypropylene, glass, and wood) without any surface pretreatment. Since porcine skin is similar to human skin tissues in terms of mechanical toughness, we chose it as the model to evaluate the tissue adhesion property of the hydrogels in our system [5]. It was observed in Fig. 4b that two pieces of porcine skins stuck together via the newly prepared PAASP-35% hydrogel film (with a contact area of 1 × 1 cm^2) could withstand 500 g loads, indicating the robust adhesiveness and the potential as adhesives for biomedical applications. To quantitatively evaluate the tissue adhesion ability of the hydrogels, the lap shear test for measurement of adhesion strength in Fig. 4c was conducted [12]. The lap-shear adhesion curves and corresponding adhesion strength of the PAASP hydrogels with different monomer concentrations to porcine skins were demonstrated in Fig. 4d and e, respectively. Overall, the adhesion strength gradually increased with the increment of monomer concentrations, and it reached 120 kPa when the concentration of AASP was 40%, which was comparable to hydrogel tissue adhesive by virtue of covalent bonding [38]. Nevertheless, the confined mobility of the polymer chain for PAASP hydrogel with the concentration of 45% led to decrease contact of the hydrogel to the substrate, causing a rapid decline in adhesion strength. Afterward, we compared the adhesion strength of PAASP-35% hydrogel with PAGLU-35%, PAAMI-35% hydrogels, and fibrin glue (FG, a commercial wound sealant). As shown in Fig. 4f and g, the adhesion strength of PAASP-35% hydrogel was as high as 106 kPa, which was 2.6, 5.3, and 8.0 times higher than that of PAGLU-35%, PAAMI-35% hydrogels, and fibrin glue, respectively. Double peeling test was further conducted to assess interfacial toughness of the PAASP hydrogels (Figs. S7a and S7b). The same trend as the adhesion strength was detected for the calculated interfacial toughness, and PAASP-35% hydrogel mediated the highest interfacial toughness of 280 J m^{-2}. Moreover, as shown in Figs. S8a and S8b, we found that the interfacial toughness increased to 350 J m^{-2} when the concentration of AASP was as high as 40%, which was obviously better than that of the commercialized medical adhesive [39]. In addition, to further highlight the

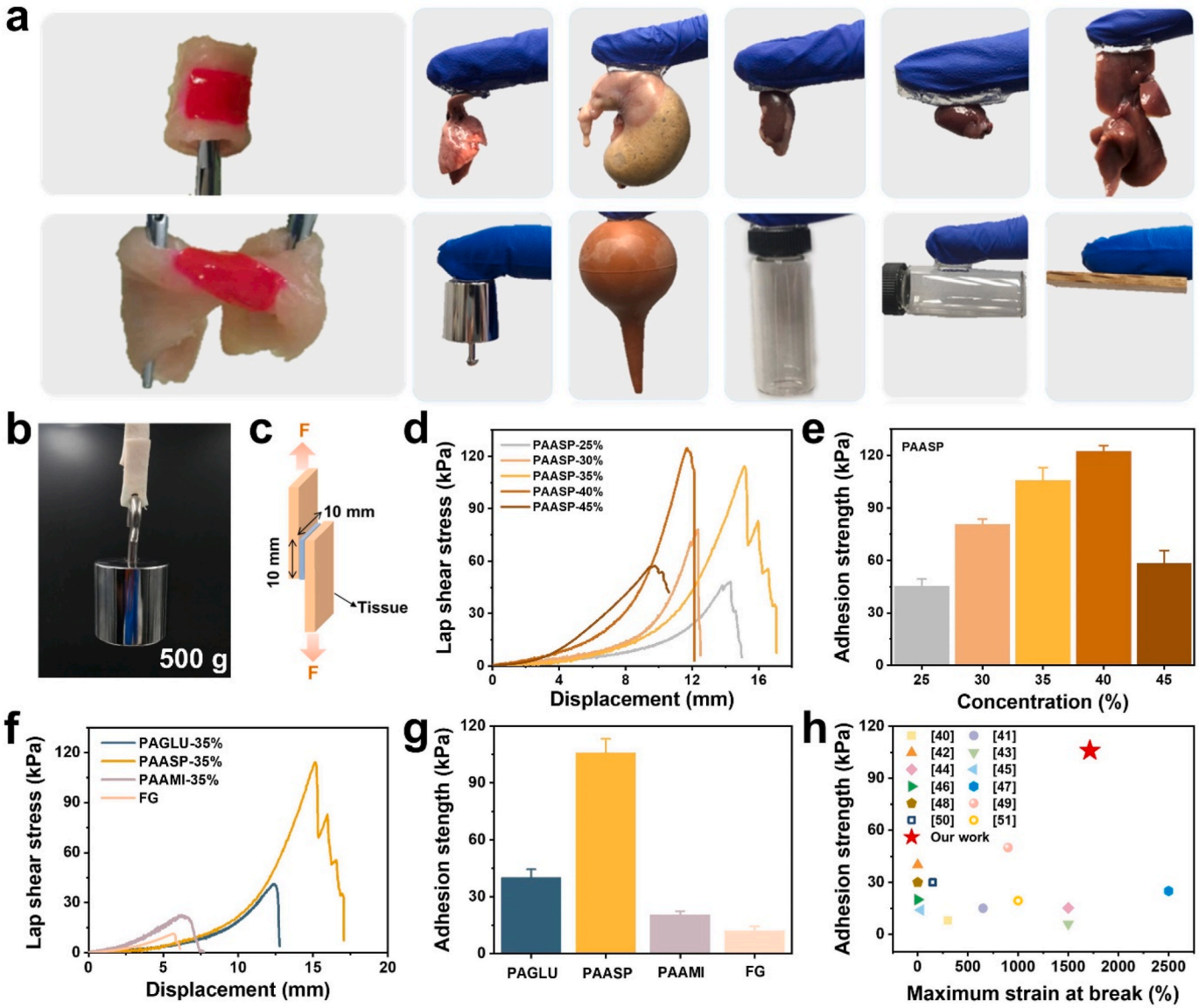

Fig. 4. Adhesion properties of PAASP hydrogels. (a) Photographs of PAASP-35% hydrogel adhering to diverse biological tissues including muscle, lung, stomach, kidney, heart, liver and various materials including iron, rubber, polypropylene (PP), glass, and wood. (b) Photograph demonstrating two porcine skins bonded by PAASP-35% hydrogel (bonding area: 1 × 1 cm^2) withstanding 500 g weight. (c) Schematic diagram for lap shear test. (d) The lap-shear adhesion curves and (e) the corresponding adhesion strength of PAASP hydrogels to porcine skin with different monomer concentrations. (f) The lap-shear adhesion curves and (g) the corresponding adhesion strength to porcine skin for PAGLU-35%, PAASP-35%, PAAMI-35% hydrogel, and fibrin glue (FG, a commercial wound sealant). (h) Comparison of adhesion strength to porcine skin and fracture strain of PAASP-35% hydrogel with the recently reported adhesive hydrogels.

outstanding adhesive performance and mechanical property of PAASP-35% hydrogel, a comparison of adhesion strength to porcine skin and maximum strain at break for a variety of adhesive hydrogels was presented in Fig. 4h. Compared with most existing adhesive hydrogels, the PAASP-35% hydrogel exhibited remarkable adhesive performance as well as superior stretchability [40–51].

Previous studies have shown that the optimized synergy of interface interactions and cohesion energy played a significant role in improving the adhesion performance [6]. We speculate that the excellent adhesion property of the PAASP hydrogels can be attributed to the synergy of the free carboxyl groups involved in interfacial adhesion and the carboxyl groups participating in hydrogen bonds formation in the hydrogel network. For PAGLU hydrogels, carboxyl groups (COOH-1, Table S1) involved in the formation of hydrogen bond crosslinked network were relatively low due to steric hindrance of the methylene groups, which led to the poor mechanical property. When subjected to external forces, the hydrogel matrix was fractured before the damage of the adhesion interface. On the contrary, most of the carboxyl groups in PAAMI hydrogels participated in the formation of hydrogen bonds to enhance the modulus of the hydrogel network, and thus few free carboxyl groups could interact with the adhesion interface. As for PAASP hydrogels, the synergy between the free carboxyl groups and the carboxyl groups involved in formation of hydrogen bonds was realized, which led to the optimal adhesion performance. The outstanding adhesiveness mediated by PAASP-35% was also observed with the substrates of iron sheets and ceramics (Figs. S9a–d).

3.4. Ex vivo rapid wound sealing and adhesion stability in liquid environment of the PAASP- 35% hydrogel

Tissue adhesive hydrogels show broad application prospects in wound healing, tissue repair, wearable devices, and other fields. However, the presence of oils or other hydrophobic substances in biological tissues usually reduces their adhesive ability significantly [52]. In

addition, most adhesive hydrogels may lose their adhesion due to the permeation of water molecules in liquid environment. Surprisingly, it was found that the PAASP-35% hydrogel could firmly adhere to the porcine muscle under the continuous water flow (Video S1). We further evaluated the potential applications of PAASP hydrogel for rapid wound closure using *ex vivo* porcine organ models. As illustrated in Fig. 5a, the PAASP-35% hydrogel was used as tissue sealant to seal incisions in stomach, bladder, small intestine, and trachea. Since the adhesion between the hydrogel and polytetrafluoroethylene (PTFE) pad was relatively poor compared with tissues, we attached PTFE to the other side of the hydrogel for facile manipulation. A wound (about 5 mm) was first created on the surface of the organs with a scalpel. During the sealing process, we attached the hydrogel sheet (2 × 2 cm^2) to the incision and gently pressed it, followed by the infusion of water into the organs (stomach, bladder, and small intestine). We found that the hydrogel adhered firmly to the organ's surface without any leakage after sealing, which was attributed to its excellent flexibility and adhesiveness (Videos S2–S4). Depending on the volume of water injected into the organ, the water pressure ranged from 0.59 to 0.78 kPa. To seal the trachea, after the hydrogel was attached to the incision, the trachea attached to the lung lobes was placed in water while the air was pumped with an injection volume of 50 L min^{-1}. It was observed that the hydrogel showed an excellent sealing effect on tracheal incision without any air leakage (Video S5). All of these results indicated that the PAASP-35% hydrogel features the vast potential to be used as wound sealant for emergency treatments.

Supplementary data related to this article can be found at https://doi.org/10.1016/j.bioactmat.2022.05.010.

To quantitatively assess the adhesion stability of the PAASP-35% hydrogel to biological tissues in liquid environment, we characterized the adhesion strength of the hydrogel to porcine skin tissue after immersing in water for different times. It was found that the adhesion

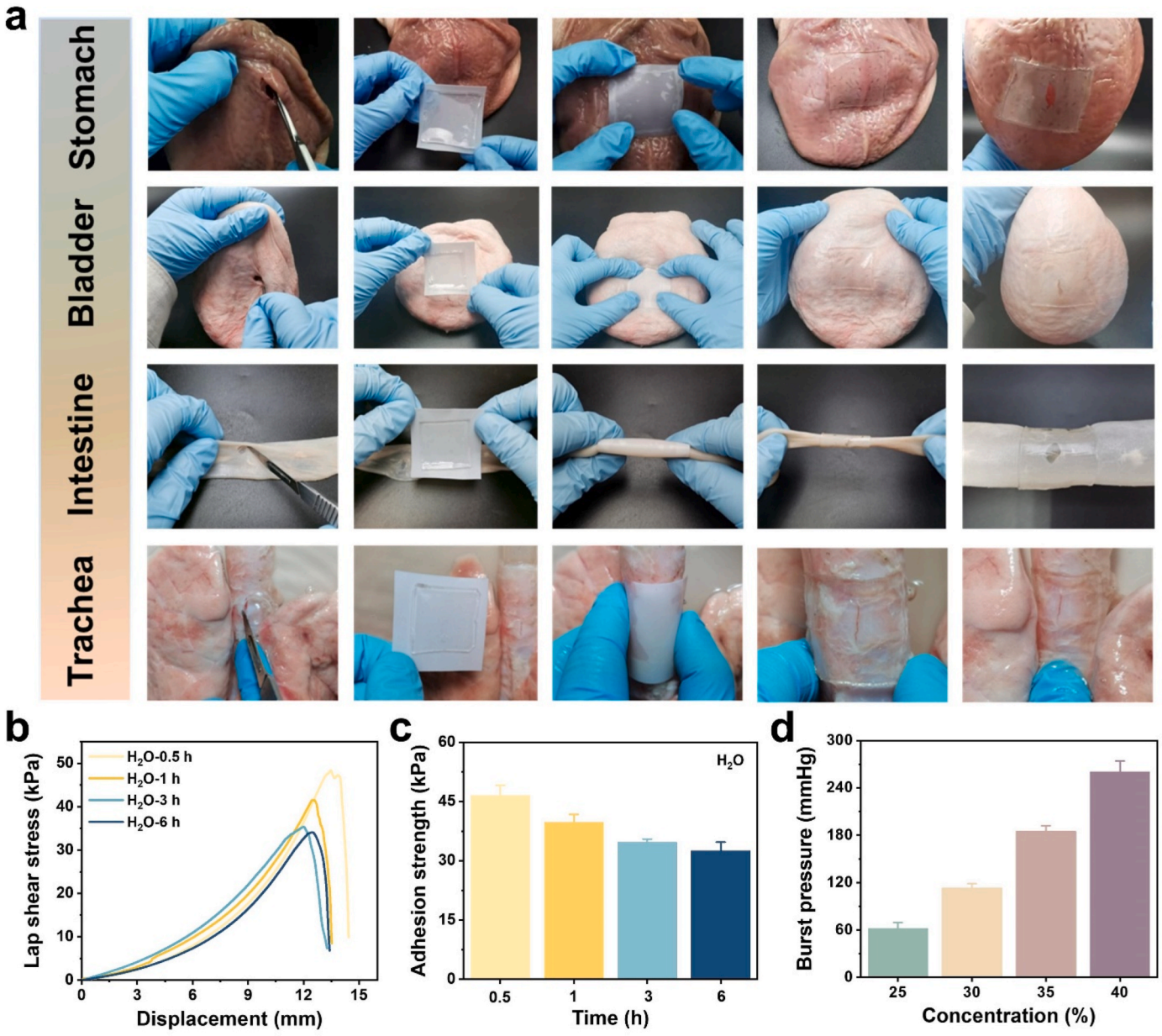

Fig. 5. The potential as wound sealants exhibited by PAASP-35% hydrogel. (a) The photographs showing the PAASP-35% hydrogel patch (2 × 2 cm^2) strongly adhering to the *ex vivo* porcine organs including stomach, bladder, intestine, and trachea to seal the incision (about 5 mm). The reverse side was bonded to polytetrafluoroethylene pad for easy operation. (b) The lap-shear adhesion curves and (c) the corresponding adhesion strength of PAASP-35% hydrogel to porcine shin after immersing in water for 0.5, 1, 3, 6 h. (d) The burst pressure of PAASP hydrogel with different monomer concentrations.

strength was 47, 40, 35, and 33 kPa, respectively, after soaking in water for 0.5, 1, 3, and 6 h (Fig. 5b and c). The variation of adhesion strength of PAASP-35% hydrogel to porcine skin in physiological saline was also characterized in Fig. S10, showing the same change trend as in water. The decrease of adhesion strength may be attributed to the network swelling and the decline of surface carboxyl group density. Although declined, the residual adhesion strength was still superior to most of the reported catechol-based adhesive hydrogels and high enough to seal the wound [36,53]. In addition, we explored the PAASP hydrogel's ability to adhere to defective tissue walls to resist the bursting pressure. The corresponding burst pressure device was depicted in Fig. S11, in which the porcine sausage shin with a 2 mm diameter hole in a chamber linked to a syringe pump was covered with PAASP-35% hydrogel to resist the pressure exerted by the syringe pump through pumping PBS. It was found in Fig. 5d that the burst pressure of PAASP-35% hydrogel reached 180 mmHg, which was better than the reported tissue sealant and normal arterial blood pressure (80–120 mmHg) indicating the potential as a hemostatic agent [19,54,55].

3.5. *In vitro Cytocompatibility, In vivo Histocompatibility and hemostatic ability of the PAASP-35% hydrogel*

Good biocompatibility is of great importance for the hydrogel to be used as bio-adhesives. The (3-(4,5-dimethyl-2-thiazoLyl)-2,5-diphenyl tetrazolium bromide (MTT) assay and Live/Dead staining were performed to evaluate the cytotoxicity of the PAASP-35% hydrogel. As shown in Fig. 6a, L929 cells cultured with hydrogel leaching solutions as high as 50 mg mL^{-1} for 3 days proliferated almost 3 times, similar to the control group (tissue culture plate). Subsequently, Live/Dead staining was also adopted to evaluate the cytotoxicity, in which green and red fluorescence represented the live and dead cells, respectively. It was observed in Fig. 6b that little red fluorescence was present in the hydrogel-treated group. The L929 cells presented the same proliferative trend and cell morphology as the control group, indicating that the hydrogel exhibited good biocompatibility. We further performed a subcutaneous implantation test to evaluate *in vivo* biocompatibility of PAASP-35% hydrogel. In Fig. 6c, the H&E staining was conducted to test the host inflammatory response of the hydrogel. Neutrophils cells were found to accumulate at the implant site after implantation for 3 days due to the acute foreign reaction. The inflammatory response was reduced after implantation for 20 days, and the tissue gradually returned to normal. Based on the above results, we can conclude that the PAASP-35% hydrogel is safe for *in vivo* applications.

Since PAASP-35% hydrogel was integrated with excellent mechanical properties, adhesion properties, and biocompatibility, it was expected to be used as wound sealant to achieve rapid hemostasis. Considering that the tissue interface was inevitably contaminated by blood or viscous mucous liquid during actual application *in vivo*, the lap shear test was performed to characterize the adhesion strength of PAASP-35% hydrogel to porcine skin coated with blood. As shown in Fig. S12, the adhesion strength was up to 30 kPa, which was desired for tissue sealing and rapid hemostasis. In addition, different biological tissue including porcine skin, gastric tissue, and intestinal mucosa were first placed at 90% humidity for 12 h, and then the adhesion performance of PAASP-35% hydrogel to wet tissue was evaluated by lap shear test. It was observed in Fig. S12 that the adhesion strength to wet porcine skin, gastric mucosa, gastric wall, and intestinal mucosa was 45, 23, 46, and 38 kPa, respectively, demonstrating great potential of adhesion to dynamic wet biological tissue for wound sealing. The mouse liver incision model, liver trauma model, and tail amputation model were established to examine the *in vivo* hemostatic property of the PAASP-35% hydrogel (Fig. 6d–f) [56]. In the process of hemostasis, the hydrogel was placed to cover the bleeding site, and a filter paper was used for absorbing the blood to quantify the hemostatic activity. The blood loss collected by the filter paper on the hemorrhaging sites was recorded every 15 s. It was found that the bloodstains of hydrogel-treated groups in three models were inconspicuous compared with control group. In addition, we also performed quantitative analysis on the final blood loss of the three models (Fig. 6g). It was illustrated in mouse liver incision model that the total blood loss of hydrogel-treated group (about 88 mg) was much less than that of control group (about 801 mg), which was consistent with intuitive results. In the mouse liver trauma model and the mouse tail amputation model, the hydrogel dramatically reduced the blood loss to 45 ± 6.5 mg and 12 ± 2.3 mg, respectively, while the untreated group presented severe blood loss of 479 ± 13.3 mg and 87 ± 6.5 mg. The outstanding *in vivo* hemostatic ability could be attributed to the strong adhesion property of the PAASP-35% hydrogel, which can serve as a robust physical barrier to prevent blood loss. These results demonstrated its potential to be used for self-rescue in emergencies.

3.6. *Adhesion stability of the PAASP-35% hydrogel under physiological conditions and paper-based Fe^{3+} transfer printing method for preparation of the PAASP-35%/Fe^{3+} Janus hydrogel patch*

Gastric perforation is one of the most common diseases in digestive system, which can cause the leakage of gastric fluid into abdomen, abdominal adhesion, bacterial peritonitis, and even death [37,57]. Surgical suture is usually used in clinic for the treatment of gastric perforation, which can cause secondary damage to the tissue. Moreover, the operation time is also not suitable in emergencies [18]. Considering the highly acidic environment of the stomach, it is necessary to design a stable and acid-resistant adhesive for gastric perforation repair. To ensure normal gastric peristalsis and avoid anastomotic zone contraction, an optimal sealant for gastric perforation treatment should possess robust elasticity, fatigue resistance, and flexibility [58]. Based on the outstanding mechanical performances, robust tissue adhesiveness, good biocompatibility, and remarkable hemostatic properties, we suspect that the PAASP-35% hydrogel may be a good candidate as tissue sealant in the gastric perforation treatment. In order to demonstrate the stability of hydrogels in acidic environment, we recorded the swelling behavior of PAASP-35% hydrogel in simulated gastric fluid at 37 °C. It was noted in Fig. S13 that the swelling ratio was about 400%, and the hydrogel could maintain stability in the simulated gastric fluid for seven days. To avoid secondary damage caused by postoperative adhesions, we prepared a Janus hydrogel by single-sided patterning with Fe^{3+} through a paper-based transfer printing method (Fig. 7a). Specifically, the filter paper was cut into the size of the hydrogel and soaked in $FeCl_3$ solution. Then, the filter paper containing Fe^{3+} was placed on one side of the hydrogel for a few seconds. In the process of transfer printing, Fe^{3+} coordinated with carboxyl groups, and the number of the free carboxyl groups interacting with tissue decreased correspondingly, which led to the decline of the adhesiveness and the prevention of abdominal adhesion (Fig. 7b). The distribution of ferric ions on both sides of the hydrogel was analyzed by surface energy spectrum analysis. Based on the results in Figs. S14a–d, the ferric ion concentration was higher on the transfer printing side, while it was basically not observed on the opposite side. Moreover, we found that the iron-permeating side could be easily peeled off from the porcine skin compared to the robust adhesiveness of the reverse side as shown in Fig. 7c and Video S6. The adhesion strength of the PAASP-35%/Fe^{3+} hydrogel was only 7.9 kPa (Fig. 7d), which was significantly lower than that of PAASP-35% hydrogel. These results demonstrated that the Janus hydrogel could realize selective adhesion for *in vivo* applications. Furthermore, we also recorded the swelling behavior of PAASP-35%/Fe^{3+} Janus hydrogel soaked in simulated gastric fluid for 1, 6, 12, and 24 h to evaluate the stability in simulated physiological environment. It was observed from Fig. S15a that the hydrogel curled due to antisymmetric swelling in simulated gastric fluid. This could be explained as the increase of crosslinking density on the Fe^{3+} transfer printing side resulting in enhanced network hardness and reduced swelling rate. Meanwhile, after soaking in simulated gastric fluid for 24 h, the hydrogel could still firmly

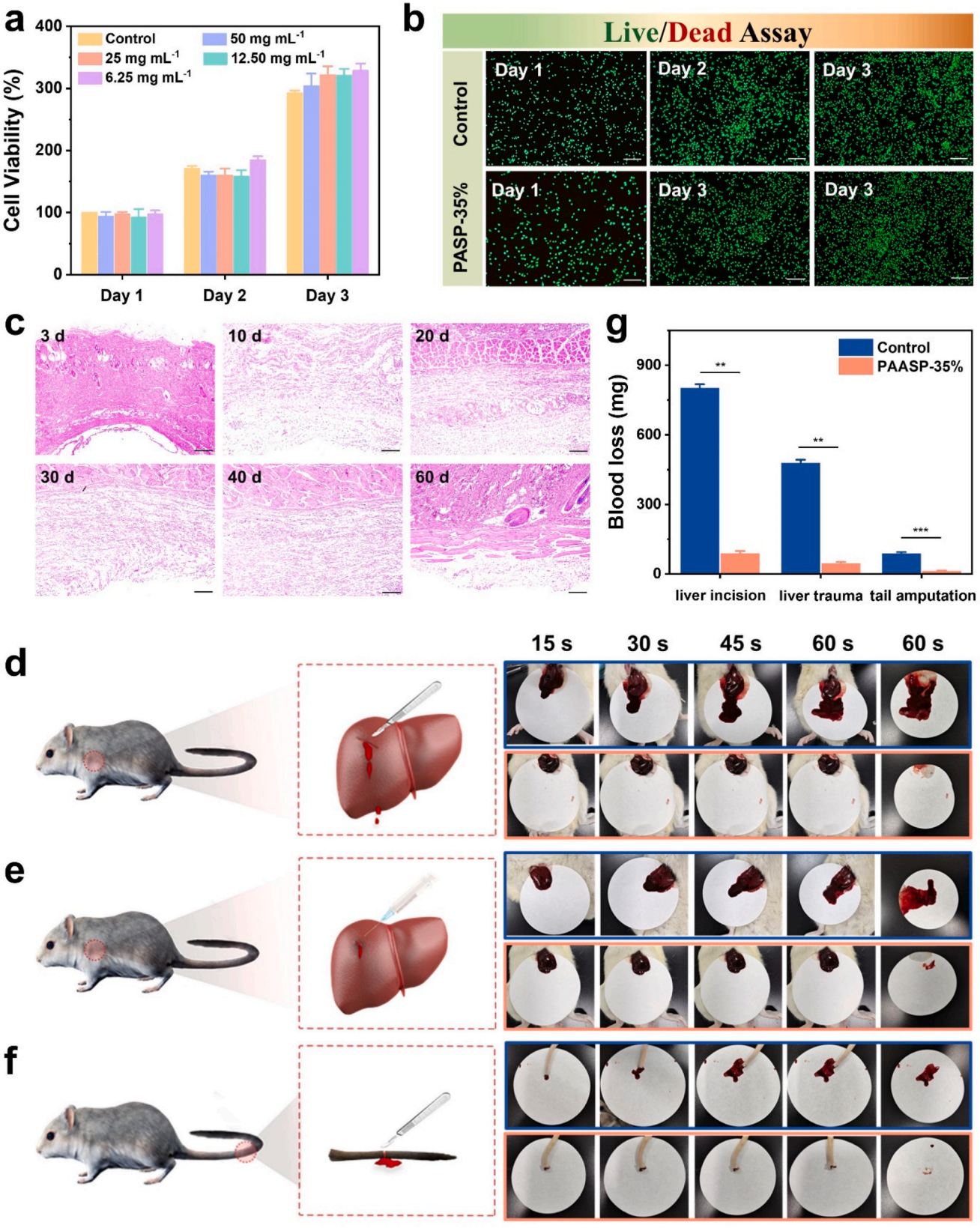

Fig. 6. The biocompatibility and *in vivo* hemostasis property of PAASP-35% hydrogel. (a) Cell viability of L929 cells cultured with the extraction of PAASP-35% hydrogels, and non-treated cells were used as a control. (b) Live/Dead staining of L929 cells cultured with the extraction of PAASP-35% hydrogels for 3 days. Scale bar: 250 μm. (c) Images of H&E staining after subcutaneous implantation of PAASP-35% hydrogel for 3, 10, 20, 30, 40, and 60 days. Scale bar: 250 μm. (d–f) Schematic pictures of mouse liver incision model, mouse liver trauma model, mouse tail amputation model and the corresponding bloodstain on filter paper in hydrogel-treated group and blank group at predetermined time intervals (15, 30, 45, and 60 s). (g) Quantitative analysis of the final blood loss in three hemorrhagic models. Mean ± SD (n = 3). *P < 0.05, **P < 0.01, ***P < 0.001.

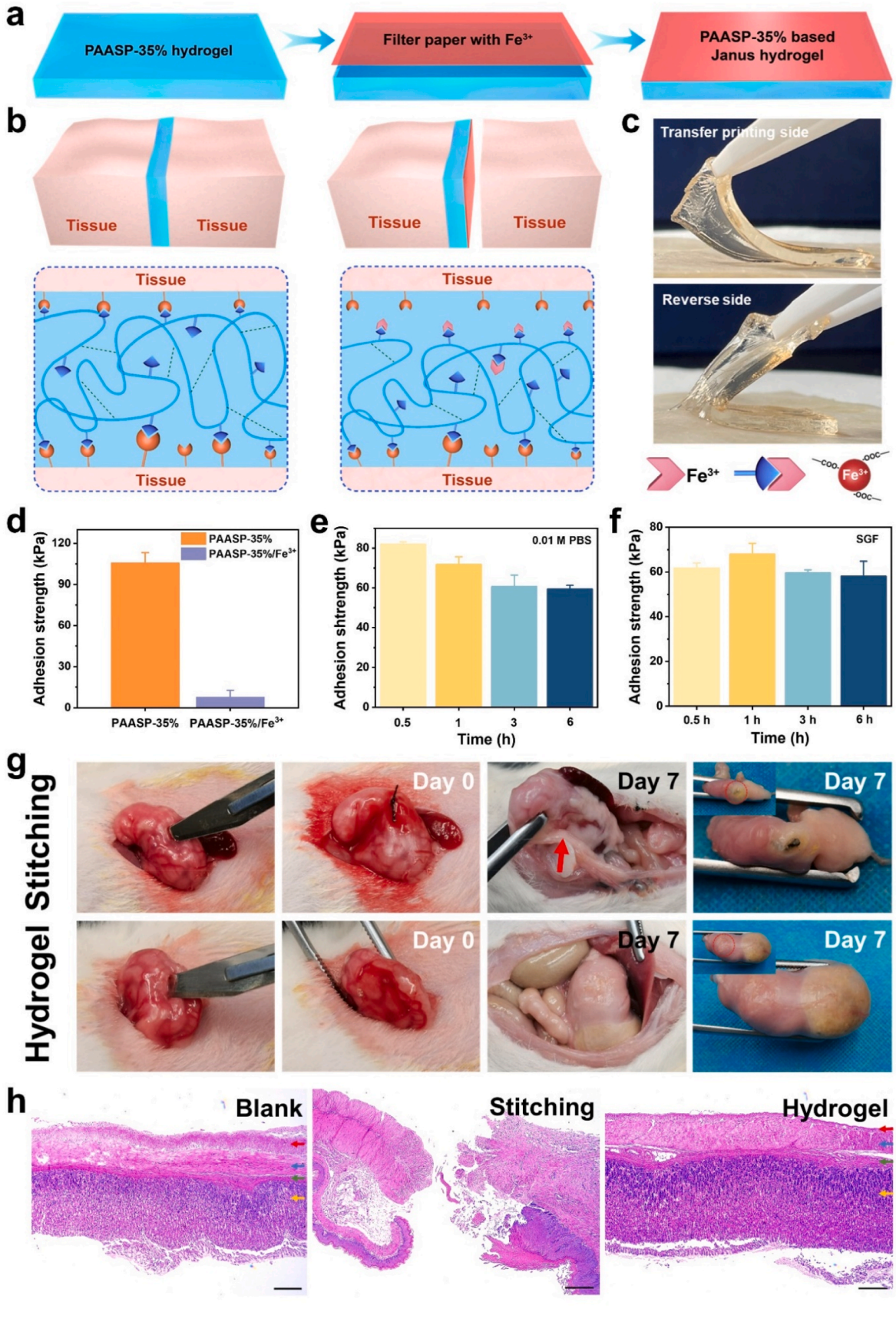

(caption on next page)

Fig. 7. The Janus hydrogel patch employed as tissue adhesive and anti-operation adhesion physical barrier for gastric perforation repair. (a) Schematic illustrations of Janus hydrogel patch prepared by paper-based Fe^{3+} transfer printing. (b) Schematic comparison between PAASP-35% hydrogel and PAASP-35% based Janus hydrogel. The transfer printing side showed no adhesion to tissue owing to the coordination between Fe^{3+} and carboxyl group. (c) Photographs showing the adhesion behavior of the transfer printing side and the reverse side to porcine skin. (d) The comparison of adhesion strength to porcine skin between PAASP-35% and PAASP-35%/Fe^{3+} hydrogels. (e) The adhesion strength of PAASP-35% hydrogel to porcine skin after immersing in PBS and (f) simulated gastric fluid for 0.5, 1, 3, 6 h at 37 °C. (g) Photographs showing the establishment of gastric perforation model on mouse (a 5 mm incision was cut on the stomach using scalpel), treatment by the Janus hydrogel patch and surgical suture, and the healing effect *in vivo* and *in vitro* at 7 days after surgery. The red arrow in suture group indicates the location of the postoperative adhesions. (h) H&E staining of normal gastric tissue (blank) and gastric perforation sections at day 7 after surgery using the Janus hydrogel and surgical suture. The red, blue, green, and golden arrows in the blank and hydrogel group represent the serosa, muscularis, submucosa, and mucosa respectively. Scale bar: 250 μm.

adhere to porcine skin under the water flushing, indicating that the hydrogel exhibited good adhesion stability in simulated body fluids (Fig. S15b). In order to simulate the complex abdominal environment, we also tested the variation of the adhesion strength of the PAASP-35% hydrogel to porcine skin in PBS and simulated gastric fluid at 37 °C. Fig. 7e illustrated that the adhesion strength to porcine skin was 82, 71, 60, 59 kPa after immersing in PBS for 0.5, 1, 3, and 6 h, respectively, which was 78, 67, 57, and 56% of the primary adhesion strength. Meanwhile, the adhesion strength was measured to be 62, 68, 60, and 58 kPa, respectively, after exposure to simulated gastric fluid (SGF) for the same time (Fig. 7f). The corresponding lap-shear adhesion curves were presented in Figs. S16a and S16b. The preservation of adhesiveness under abdominal and gastric conditions is beneficial to practical applications for the treatment of gastric perforation.

Supplementary data related to this article can be found at https://doi.org/10.1016/j.bioactmat.2022.05.010.

3.7. *In vivo* gastric perforation repair by PAASP-35%/Fe^{3+} Janus hydrogel patch

To verify the treatment efficiency in gastric perforation, we employed the Janus hydrogel as tissue adhesive to promote the healing of stomach incision on mice. As shown in Fig. 7g, an incision with a length of 0.5 cm was created on the mice's stomach using a scalpel, which was treated with the Janus hydrogel patch and suture, respectively. In the hydrogel-treated group, the incision was first gently wiped with a cotton swab and then quickly sealed with the Janus hydrogel patch (1 cm in diameter). The operation process was recorded in Video S7. It was found that the incision in the hydrogel-treated group healed efficiently one week after surgery, and the surface of the stomach was smooth without tissue adhesion. However, severe tissue adhesion appeared in the suture group, which may be due to the leakage of the gastric fluid and the inflammatory reaction. In addition, the stomach was also isolated to examine the morphology and integrity. The gastric fluid flowed out under the external force in the suture group, indicating the frustrated healing efficiency. In contrast, the incision in the hydrogel-treated group was completely healed, and the stomach remained in normal shape without any leakage. These results could be attributed to the Janus hydrogel patch being a potent biological interface for simultaneous wound repair and anti-adhesion. Hematoxylin and eosin (H&E) staining was further conducted to evaluate the therapeutic sealing effect. It was presented in Fig. 7h that the gastric wall structure was destroyed, and the tissues were discontinuous in the sutured group, while the typical three-layer gastric wall structure was restored in the hydrogel-treated group, which was similar to the normal gastric tissue. Hence, we can conclude that the PAASP-35%/Fe^{3+} hydrogel could be an excellent candidate to be used as a tissue patch for gastric perforation healing.

Supplementary data related to this article can be found at https://doi.org/10.1016/j.bioactmat.2022.05.010.

4. Conclusion

In conclusion, we fabricated three kinds of hydrogen bond cross-linked hydrogels by one-step free radical polymerization of three bi-carboxyl-included acrylamide monomers. Experimental verification and simulation calculation simultaneously revealed that the PAASP hydrogel realized synergistic effect between the interface interaction and bulk toughness, thus exhibiting the best adhesion properties. The PAASP hydrogel not only realized the combination of excellent stretchability, toughness, elasticity, and fatigue resistance but also showed strong adhesion to biological tissues. Encouragingly, the adhesion strength of PAASP hydrogel to tissues remained stable for a long time in simulated body fluids. *Ex vivo* porcine organ models demonstrated that the PAASP hydrogel had the potential to seal tissue incision in emergencies. In addition, the PAASP hydrogel also possessed good biocompatibility and rapid hemostasis ability. The prepared Janus hydrogels with completely different double-sided properties by simple paper-based ion transfer printing could act as tissue sealants to promote wound healing and physical barriers to prevent post-operation adhesion simultaneously for the treatment of gastric perforation on mice. It is convinced that PAASP hydrogel could provide a new option for *in vivo* applications, including rapid hemostasis, wound closure, and tissue repair.

Conflict of interest

The authors declare no conflict of interest.

Ethics approval and consent to participate

All animal experiments in this study were approved by the Ethics Committee of Xi'an Jiaotong University.

CRediT authorship contribution statement

Jing Yu: Conceptualization, Methodology, Validation, Formal analysis, Writing – original draft. **Yanyang Qin:** Formal analysis, Investigation, Software. **Yuxuan Yang:** Investigation, Formal analysis. **Xiaodan Zhao:** Investigation, Formal analysis. **Zixi Zhang:** Supervision. **Qiang Zhang:** Supervision. **Yaqiong Su:** Formal analysis, Software. **Yanfeng Zhang:** Supervision. **Yilong Cheng:** Conceptualization, Supervision, Writing – review & editing, Supervision, Project administration.

Declaration of competing interest

The authors declare that they have no known competing financial interests or personal relationships that could have appeared to influence the work reported in this paper.

Acknowledgements

We thank Mr. Zijun Ren and Ms. Jiamei Liu at Instrument Analysis Center of Xi'an Jiaotong University for their assistance with scanning electron microscope (SEM) test and X-ray photoelectron spectroscopy (XPS) analysis. This study was funded by the National Natural Science Foundation of China (NSFC 52173139), the Shaanxi International Science and Technology Cooperation Program Project (2020KW-062), the "Young Talent Support Plan" of Xi'an Jiaotong University, and

Fundamental Research Funds for the Central Universities (xzy022021040). This work was also supported by the Opening Research Fund from Key Laboratory of Shaanxi Province for Craniofacial Precision Medicine Research, College of Stomatology, Xi'an Jiaotong University (2021LHM-KFKT003).

Appendix A. Supplementary data

Supplementary data to this article can be found online at https://doi.org/10.1016/j.bioactmat.2022.05.010.

References

[1] X. Zhao, Y. Liang, Y. Huang, J. He, Y. Han, B. Guo, Physical double-network hydrogel adhesives with rapid shape adaptability, fast self-healing, antioxidant and NIR/pH stimulus-responsiveness for multidrug-resistant bacterial infection and removable wound dressing, Adv. Funct. Mater. 30 (2020) 1910748, https://doi.org/10.1002/adfm.201910748.

[2] M.M. Hasani-Sadrabadi, P. Sarrion, S. Pouraghaei, Y. Chau, S. Ansari, S. Li, T. Aghaloo, A. Moshaverinia, An engineered cell-laden adhesive hydrogel promotes craniofacial bone tissue regeneration in rats, Sci. Transl. Med. 12 (2020), eaay6853, https://doi.org/10.1126/scitranslmed.aay6853.

[3] J. Chen, D. Wang, L.H. Wang, W. Liu, A. Chiu, K. Shariati, Q. Liu, X. Wang, Z. Zhong, J. Webb, R.E. Schwartz, N. Bouklas, M. Ma, An adhesive hydrogel with "Load-Sharing" effect as tissue bandages for drug and cell delivery, Adv. Mater. 32 (2020) 2001628, https://doi.org/10.1002/adma.202001628.

[4] C. Xie, X. Wang, H. He, Y. Ding, X. Lu, Mussel-inspired hydrogels for self-adhesive bioelectronics, Adv. Funct. Mater. 30 (2020) 1909954, https://doi.org/10.1002/adfm.201909954.

[5] J. Li, A.D. Celiz, J. Yang, Q. Yang, I. Wamala, W. Whyte, B.R. Seo, N.V. Vasilyev, J. J. Vlassak, Z. Suo, D.J. Mooney, Tough adhesives for diverse wet surfaces, Science 357 (2017) 378–381, https://doi.org/10.1126/science.aah6362.

[6] J. Yang, R. Bai, B. Chen, Z. Suo, Hydrogel adhesion: a supramolecular synergy of chemistry, topology, and mechanics, Adv. Funct. Mater. 30 (2019) 1901693, https://doi.org/10.1002/adfm.201901693.

[7] Y. Gao, J. Chen, X. Han, Y. Pan, P. Wang, T. Wang, T. Lu, A universal strategy for tough adhesion of wet soft material, Adv. Funct. Mater. 30 (2020) 2003207, https://doi.org/10.1002/adfm.202003207.

[8] Q. Chen, L. Zhu, H. Chen, H. Yan, L. Huang, J. Yang, J. Zheng, A novel design strategy for fully physically linked double network hydrogels with tough, fatigue resistant, and self-healing properties, Adv. Funct. Mater. 25 (2015) 1598–1607, https://doi.org/10.1002/adfm.201404357.

[9] N. Rauner, M. Meuris, M. Zoric, J.C. Tiller, Enzymatic mineralization generates ultrastiff and tough hydrogels with tunable mechanics, Nature 543 (2017) 407–410, https://doi.org/10.1038/nature21392.

[10] Y. Bu, L. Zhang, G. Sun, F. Sun, J. Liu, F. Yang, P. Tang, D. Wu, Tetra-PEG based hydrogel sealants for in vivo visceral hemostasis, Adv. Mater. 31 (2019) 1901580, https://doi.org/10.1002/adma.201901580.

[11] C. Liu, N. Morimoto, L. Jiang, S. Kawahara, T. Noritomi, H. Yokoyama, K. Mayumi, K. Ito, Tough hydrogels with rapid self-reinforcement, Science 372 (2021) 1078–1081, https://doi.org/10.1126/science.aaz6694.

[12] C. Cui, T. Wu, F. Gao, C. Fan, Z. Xu, H. Wang, B. Liu, W. Liu, An autolytic high strength instant adhesive hydrogel for emergency self-rescue, Adv. Funct. Mater. 28 (2018) 1804925, https://doi.org/10.1002/adfm.201804925.

[13] N. Annabi, Y.-N. Zhang, A. Assmann, E.S. Sani, G. Cheng, A.D. Lassaletta, A. Vegh, B. Dehghani, G.U. Ruiz-Esparza, X. Wang, S. Gangadharan, A.S. Weiss, A. Khademhosseini, Engineering a highly elastic human protein-based sealant for surgical applications, Sci. Transl. Med. 9 (2017) eaai7466.

[14] P. Rao, T.L. Sun, L. Chen, R. Takahashi, G. Shinohara, H. Guo, D.R. King, T. Kurokawa, J.P. Gong, Tough hydrogels with fast, strong, and reversible underwater adhesion based on a multiscale design, Adv. Mater. 30 (2018) 1801884, https://doi.org/10.1002/adma.201801884.

[15] L. Han, M. Wang, L.O. Prieto-López, X. Deng, J. Cui, Self-hydrophobization in a dynamic hydrogel for creating nonspecific repeatable underwater adhesion, Adv. Funct. Mater. 30 (2019) 1907064, https://doi.org/10.1002/adfm.201907064.

[16] A. Shagan, W. Zhang, M. Mehta, S. Levi, D.S. Kohane, B. Mizrahi, Hot glue gun releasing biocompatible tissue adhesive, Adv. Funct. Mater. 30 (2020) 1900998, https://doi.org/10.1002/adfm.201900998.

[17] C. Cui, T. Wu, X. Chen, Y. Liu, Y. Li, Z. Xu, C. Fan, W. Liu, A Janus hydrogel wet adhesive for internal tissue repair and anti-postoperative adhesion, Adv. Funct. Mater. 30 (2020) 2005689, https://doi.org/10.1002/adfm.202005689.

[18] G.M. Taboada, K. Yang, M.J.N. Pereira, S.S. Liu, Y. Hu, J.M. Karp, N. Artzi, Y. Lee, Overcoming the translational barriers of tissue adhesives, Nat. Rev. Mater. 5 (2020) 310–329, https://doi.org/10.1038/s41578-019-0171-7.

[19] A.H.C. Anthis, X. Hu, M.T. Matter, A.L. Neuer, K. Wei, A.A. Schlegel, F.H. L. Starsich, I.K. Herrmann, Chemically stable, strongly adhesive sealant patch for intestinal anastomotic leakage prevention, Adv. Funct. Mater. 31 (2021) 2007099, https://doi.org/10.1002/adfm.202007099.

[20] L. Han, X. Lu, K. Liu, K. Wang, L. Fang, L.T. Weng, H. Zhang, Y. Tang, F. Ren, C. Zhao, G. Sun, R. Liang, Z. Li, Mussel-inspired adhesive and tough hydrogel based on nanoclay confined dopamine polymerization, ACS Nano 11 (2017) 2561–2574, https://doi.org/10.1021/acsnano.6b05318.

[21] R. Wang, J. Li, W. Chen, T. Xu, S. Yun, Z. Xu, Z. Xu, T. Sato, B. Chi, H. Xu, A biomimetic mussel-inspired ε-Poly-l-lysine hydrogel with robust tissue-anchor and anti-infection capacity, Adv. Funct. Mater. 27 (2017) 1604894, https://doi.org/10.1002/adfm.201604894.

[22] J. Shin, S. Choi, J.H. Kim, J.H. Cho, Y. Jin, S. Kim, S. Min, S.K. Kim, D. Choi, S. W. Cho, Tissue tapes-phenolic hyaluronic acid hydrogel patches for off-the-shelf therapy, Adv. Funct. Mater. 29 (2019) 1903863, https://doi.org/10.1002/adfm.201903863.

[23] J. Saiz-Poseu, J. Mancebo-Aracil, F. Nador, F. Busque, D. Ruiz-Molina, The chemistry behind catechol-based adhesion, Angew. Chem. Int. Ed. Engl. 58 (2019) 696–714, https://doi.org/10.1002/anie.201801063.

[24] Q. Guo, J. Chen, J. Wang, H. Zeng, J. Yu, Recent progress in synthesis and application of mussel-inspired adhesives, Nanoscale 12 (2020) 1307–1324, https://doi.org/10.1039/c9nr09780e.

[25] J.H. Ryu, Y. Lee, W.H. Kong, T.G. Kim, T.G. Park, H. Lee, Catechol-functionalized chitosan/pluronic hydrogels for tissue adhesives and hemostatic materials, Biomacromolecules 12 (2011) 2653–2659, https://doi.org/10.1021/bm200464x.

[26] J. Shin, J.S. Lee, C. Lee, H.-J. Park, K. Yang, Y. Jin, J.H. Ryu, K.S. Hong, S.-H. Moon, H.-M. Chung, H.S. Yang, S.H. Um, J.-W. Oh, D.-I. Kim, H. Lee, S.-W. Cho, Tissue adhesive catechol-modified hyaluronic acid hydrogel for effective, minimally invasive cell therapy, Adv. Funct. Mater. 25 (2015) 3814–3824, https://doi.org/10.1002/adfm.201500006.

[27] Y. Liu, H. Meng, S. Konst, R. Sarmiento, R. Rajachar, B.P. Lee, Injectable dopamine-modified poly(ethylene glycol) nanocomposite hydrogel with enhanced adhesive property and bioactivity, ACS Appl. Mater. Interfaces 6 (2014) 16982–16992, https://doi.org/10.1021/am504566v.

[28] G. He, X. Yan, Z. Miao, H. Qian, Y. Ma, Y. Xu, L. Gao, Y. Lu, Z. Zha, Anti-inflammatory catecholic chitosan hydrogel for rapid surgical trauma healing and subsequent prevention of tumor recurrence, Chin. Chem. Lett. 31 (2020) 1807–1811, https://doi.org/10.1016/j.cclet.2020.02.032.

[29] X. Hu, M. Vatankhah-Varnoosfaderani, J. Zhou, Q. Li, S.S. Sheiko, Weak hydrogen bonding enables hard, strong, tough, and elastic hydrogels, Adv. Mater. 27 (2015) 6899–6905, https://doi.org/10.1002/adma.201503724.

[30] J. Kang, D. Son, G.N. Wang, Y. Liu, J. Lopez, Y. Kim, J.Y. Oh, T. Katsumata, J. Mun, Y. Lee, L. Jin, J.B. Tok, Z. Bao, Tough and water-insensitive self-healing elastomer for robust electronic skin, Adv. Mater. 30 (2018) 1706846, https://doi.org/10.1002/adma.201706846.

[31] F. Gao, Y. Zhang, Y. Li, B. Xu, Z. Cao, W. Liu, Sea cucumber-inspired autolytic hydrogels exhibiting tunable high mechanical performances, repairability, and reusability, ACS Appl. Mater. Interfaces 8 (2016) 8956–8966, https://doi.org/10.1021/acsami.6b00912.

[32] J. Yu, K. Xu, X. Chen, X. Zhao, Y. Yang, D. Chu, Y. Xu, Q. Zhang, Y. Zhang, Y. Cheng, Highly stretchable, tough, resilient, and antifatigue hydrogels based on multiple hydrogen bonding interactions formed by phenylalanine derivatives, Biomacromolecules 22 (2021) 1297–1304, https://doi.org/10.1021/acs.biomac.0c01788.

[33] Y. Gao, F. Jia, G. Gao, Transparent and conductive amino acid-tackified hydrogels as wearable strain sensors, Chem. Eng. J. 375 (2019) 121915, https://doi.org/10.1016/j.cej.2019.121915.

[34] X. Peng, Y. Li, Q. Zhang, C. Shang, Q.-W. Bai, H. Wang, Tough hydrogels with programmable and complex shape deformations by ion dip-dyeing and transfer printing, Adv. Funct. Mater. 26 (2016) 4491–4500, https://doi.org/10.1002/adfm.201601389.

[35] X. Zhou, T. Li, J. Wang, F. Chen, D. Zhou, Q. Liu, B. Li, J. Cheng, X. Zhou, B. Zheng, Mechanochemical regulated origami with tough hydrogels by ion transfer printing, ACS Appl. Mater. Interfaces 10 (2018) 9077–9084, https://doi.org/10.1021/acsami.8b01610.

[36] X. Su, Y. Luo, Z. Tian, Z. Yuan, Y. Han, R. Dong, L. Xu, Y. Feng, X. Liu, J. Huang, Ctenophore-inspired hydrogels for efficient and repeatable underwater specific adhesion to biotic surfaces, Mater. Horiz. 7 (2020) 2651–2661, https://doi.org/10.1039/d0mh01344g.

[37] Z. Ma, G. Bao, J. Li, Multifaceted design and emerging applications of tissue adhesives, Adv. Mater. 33 (2021) 2007663, https://doi.org/10.1002/adma.202007663.

[38] H. Yuk, C.E. Varela, C.S. Nabzdyk, X. Mao, R.F. Padera, E.T. Roche, X. Zhao, Dry double-sided tape for adhesion of wet tissues and devices, Nature 575 (2019) 169–174, https://doi.org/10.1038/s41586-019-1710-5.

[39] E. Lih, J.S. Lee, K.M. Park, K.D. Park, Rapidly curable chitosan-PEG hydrogels as tissue adhesives for hemostasis and wound healing, Acta Biomater. 8 (2012) 3261–3269, https://doi.org/10.1016/j.actbio.2012.05.001.

[40] L. Teng, Y. Chen, M. Jin, Y. Jia, Y. Wang, L. Ren, Weak hydrogen bonds lead to self-healable and bioadhesive hybrid polymeric hydrogels with mineralization-active functions, Biomacromolecules 19 (2018) 1939–1949, https://doi.org/10.1021/acs.biomac.7b01688.

[41] X. He, L. Liu, H. Han, W. Shi, W. Yang, X. Lu, Bioinspired and microgel-tackified adhesive hydrogel with rapid self-healing and high stretchability, Macromolecules 52 (2018) 72–80, https://doi.org/10.1021/acs.macromol.8b01678.

[42] S. Hong, D. Pirovich, A. Kilcoyne, C.H. Huang, H. Lee, R. Weissleder, Supramolecular metallo-bioadhesive for minimally invasive use, Adv. Mater. 28 (2016) 8675–8680, https://doi.org/10.1002/adma.201602606.

[43] T. Chen, Y. Chen, H.U. Rehman, Z. Chen, Z. Yang, M. Wang, H. Li, H. Liu, Ultratough, self-healing, and tissue-adhesive hydrogel for wound dressing, ACS Appl. Mater. Interfaces 10 (2018) 33523–33531, https://doi.org/10.1021/acsami.8b10064.

[44] X. Jing, H.Y. Mi, Y.J. Lin, E. Enriquez, X.F. Peng, L.S. Turng, Highly stretchable and biocompatible strain sensors based on mussel-inspired super-adhesive self-healing

hydrogels for human motion monitoring, ACS Appl. Mater. Interfaces 10 (2018) 20897–20909, https://doi.org/10.1021/acsami.8b06475.
[45] H. Jung, M.K. Kim, J.Y. Lee, S.W. Choi, J. Kim, Adhesive hydrogel patch with enhanced strength and adhesiveness to skin for transdermal drug delivery, Adv. Funct. Mater. 30 (2020) 2004407, https://doi.org/10.1002/adfm.202004407.
[46] L. Wang, X. Zhang, K. Yang, Y.V. Fu, T. Xu, S. Li, D. Zhang, L.N. Wang, C.S. Lee, A novel double-crosslinking-double-network design for injectable hydrogels with enhanced tissue adhesion and antibacterial capability for wound treatment, Adv. Funct. Mater. 30 (2020) 1904156, https://doi.org/10.1002/adfm.201904156.
[47] D. Gan, W. Xing, L. Jiang, J. Fang, C. Zhao, F. Ren, L. Fang, K. Wang, X. Lu, Plant-inspired adhesive and tough hydrogel based on Ag-Lignin nanoparticles-triggered dynamic redox catechol chemistry, Nat. Commun. 10 (2019) 1487, https://doi.org/10.1038/s41467-019-09351-2.
[48] L. Zhou, C. Dai, L. Fan, Y. Jiang, C. Liu, Z. Zhou, P. Guan, Y. Tian, J. Xing, X. Li, Y. Luo, P. Yu, C. Ning, G. Tan, Injectable self-healing natural biopolymer-based hydrogel adhesive with thermoresponsive reversible adhesion for minimally invasive surgery, Adv. Funct. Mater. 31 (2021) 2007457, https://doi.org/10.1002/adfm.202007457.
[49] C. Shao, L. Meng, M. Wang, C. Cui, B. Wang, C.R. Han, F. Xu, J. Yang, Mimicking dynamic adhesiveness and strain-stiffening behavior of biological tissues in tough and self-healable cellulose nanocomposite hydrogels, ACS Appl. Mater. Interfaces 11 (2019) 5885–5895, https://doi.org/10.1021/acsami.8b21588.
[50] B. Liu, Y. Wang, Y. Miao, X. Zhang, Z. Fan, G. Singh, X. Zhang, K. Xu, B. Li, Z. Hu, M. Xing, Hydrogen bonds autonomously powered gelatin methacrylate hydrogels with super-elasticity, self-heal and underwater self-adhesion for sutureless skin and stomach surgery and E-skin, Biomaterials 171 (2018) 83–96, https://doi.org/10.1016/j.biomaterials.2018.04.023.
[51] X. Pei, H. Zhang, Y. Zhou, L. Zhou, J. Fu, Stretchable, self-healing and tissue-adhesive zwitterionic hydrogels as strain sensors for wireless monitoring of organ motions, Mater. Horiz. 7 (2020) 1872–1882, https://doi.org/10.1039/d0mh00361a.
[52] L. Han, L. Yan, K. Wang, L. Fang, H. Zhang, Y. Tang, Y. Ding, L.-T. Weng, J. Xu, J. Weng, Y. Liu, F. Ren, X. Lu, Tough, self-healable and tissue-adhesive hydrogel with tunable multifunctionality, NPG Asia Mater. 9 (2017) e372, https://doi.org/10.1038/am.2017.33.
[53] Z. Qiao, X. Lv, S. He, S. Bai, X. Liu, L. Hou, J. He, D. Tong, R. Ruan, J. Zhang, J. Ding, H. Yang, A mussel-inspired supramolecular hydrogel with robust tissue anchor for rapid hemostasis of arterial and visceral bleedings, Bioact. Mater. 6 (2021) 2829–2840, https://doi.org/10.1016/j.bioactmat.2021.01.039.
[54] Y. Hong, F. Zhou, Y. Hua, X. Zhang, C. Ni, D. Pan, Y. Zhang, D. Jiang, L. Yang, Q. Lin, Y. Zou, D. Yu, D.E. Arnot, X. Zou, L. Zhu, S. Zhang, H. Ouyang, A strongly adhesive hemostatic hydrogel for the repair of arterial and heart bleeds, Nat. Commun. 10 (2019) 2060, https://doi.org/10.1038/s41467-019-10004-7.
[55] Y. Liu, H. Meng, Z. Qian, N. Fan, W. Choi, F. Zhao, B.P. Lee, A moldable nanocomposite hydrogel composed of a mussel-inspired polymer and a nanosilicate as a fit-to-shape tissue sealant, Angew. Chem. Int. Ed. Engl. 56 (2017) 4224–4228, https://doi.org/10.1002/anie.201700628.
[56] J. He, M. Shi, Y. Liang, B. Guo, Conductive adhesive self-healing nanocomposite hydrogel wound dressing for photothermal therapy of infected full-thickness skin wounds, Chem. Eng. J. 394 (2020) 124888, https://doi.org/10.1016/j.cej.2020.124888.
[57] X. Xu, X. Xia, K. Zhang, A. Rai, Z. Li, P. Zhao, K. Wei, L. Zou, B. Yang, W. Wong, P. Chiu, L. Bian, Bioadhesive hydrogels demonstrating pH-independent and ultrafast gelation promote gastric ulcer healing in pigs, Sci. Transl. Med. 12 (2020), https://doi.org/10.1126/scitranslmed.aba8014 eaba8014.
[58] T. Vuocolo, R. Haddad, G.A. Edwards, R.E. Lyons, N.E. Liyou, J.A. Werkmeister, J. A. Ramshaw, C.M. Elvin, A highly elastic and adhesive gelatin tissue sealant for gastrointestinal surgery and colon anastomosis, J. Gastrointest. Surg. 16 (2012) 744–752, https://doi.org/10.1007/s11605-011-1771-8.